Received: 27 April 2023 | Revised: 30 July 2023 | Accepted: 31 July 2023

DOI: 10.1002/pol.20230264

RESEARCH ARTICLE

JOURNAL OF POLYMER SCIENCE WILEY

Pull-out behavior of polymer fibers in concrete

Michael Sigrüner[1] | **Götz Hüsken**[2] | **Stephan Pirskawetz**[2] | **Jonas Herz**[1] | **Dirk Muscat**[1] | **Nicole Strübbe**[1]

[1]Polymer Engineering Department, Faculty of Engineering Sciences, Technische Hochschule Rosenheim, Rosenheim, Germany

[2]Division 7.4 – Technology of Construction Materials, Bundesanstalt für Materialforschung und -prüfung (BAM), Berlin, Germany

Correspondence
Nicole Strübbe, Polymer Engineering Department, Faculty of Engineering Sciences, Technische Hochschule Rosenheim, Hochschulstraße 1 83024 Rosenheim, Germany.
Email: nicole.struebbe@th-rosenheim.de

Funding information
German Federal Ministry of Education and Research, Grant/Award Number: 13FH068PA6

Abstract

The bond between polymer fibers and the surrounding cementitious matrix is essential for the development of concrete reinforcement. The single fiber pull-out test (SFPT) is the standard characterization technique for testing the bond strength. However, the different phases of debonding cannot be distinguished by the SFPT. This study investigates the debonding of different polymer fibers from the surrounding cementitious matrix with a modified SFPT and proposes methods to change the SFPT setup to generate more valuable information on the debonding mechanism. The SFPT was equipped with linear variable differential transformers (LVDT), digital image correlation (DIC) and acoustic emission (AE) analysis. The results demonstrate that the modified SFPT allows a better understanding of the different phases of debonding during fiber pull-out. Furthermore, bond strength values calculated by different methods reveal that the chemical bond of the investigated polymers is not different as reported by previous studies. Deformation measurements performed using LVDTs and DIC are suitable measuring techniques to characterize the debonding mechanism in SFPT. A correlation between recorded AE and debonding phases was not found.

KEYWORDS

acoustic emission, bond behavior, polymer fibers, pull-out

1 | INTRODUCTION

Concrete is an important and widely used building material for the construction industry due to its balanced and reasonable relation between engineering properties, such as mechanical strength and durability, and economic benefits, such as handling, costs and availability of raw materials. However, the concrete itself has a low tensile strength. One solution to overcome the low tensile strength is the combination with materials that show high tensile strength. This so-called reinforcement can be realized by materials like steel bars, textiles or the addition of fibers.[1–4] In recent years, there has been an increasing interest in fiber reinforced concrete. Materials such as steel, polymers or inorganic materials have been investigated in different sizes and surface modifications.[5–10] Polymer fibers, for instance polypropylene (PP) fibers are of high interest, due to their easy handling, good workability and high economic impact.[11–13] Despite their beneficial effects, the main problem with PP fibers is the poor adhesion between the

fiber and the matrix.[6] PP is a non-polar semi-crystalline standard polymer with high chemical resistance, thermal stability and low price. The mechanical properties of PP are depending on the micro-structural orientation. The tensile strength of PP fibers is about half compared to steel fibers and the Young's modulus is smaller by a factor of 10.[14,15] However, its chemical inertness hinders the chemical bond of PP fibers with the concrete matrix. Grafting PP with silanes as done by Felix et al.,[16] Bengtson et al.,[17] Huang et al.,[18] or Nachtigall et al.[19] is assumed to result in chemical active fibers with better bond to the concrete matrix.

Xu et al.,[9] Choi et al.,[20] and Švegl et al.[21] showed that silanes as bonding agents can increase the surface interaction between concrete and a given material. Other polymers provide a higher chemical activity. Polyesters, such as polyethylene terephthalate (PET), react chemically with an alkaline environment, which leads to a partly dissolved surface or saponification.[22–24] A medium chemical attack by the alkaline pore solution on the fiber surface is a possibility to create interfacial bond. Additionally, polar polymer materials offer adhesion via second valence bonds, such as hydrogen bonds or van-der-Waals bonds, to other polar substances such as concrete.[25,26] Physical anchoring of the fiber by crimping, embossment or surface roughness in the concrete matrix is another method to establish a good fiber-matrix adhesion.[5,27,28] The characterization of the fiber-matrix adhesion is difficult, due to a multi mechanism-based fiber debonding. In literature, various methods to evaluate the micro-mechanical composite properties are mentioned.[29–32] The main problem in adhesion measurements for single fibers is the lack of consistency and methods to distinguish between the individual adhesion mechanisms. The single fiber pull-out test (SFPT) is a common method to characterize the fiber-matrix adhesion and will be used in this study to analyze polymeric fibers for concrete reinforcement.[27,33–35] Gao[36] and Hsueh[37,38] developed mathematical methods to describe the fiber-matrix debonding.

Redon et al.[39] divide the pull-out process in 3 major regimes as shown in Figure 1. First, a fiber embedded in concrete with a certain embedded length is pulled out of the concrete with a constant displacement, which results in an increasing pull-out force F. The fiber embedded end is not moving and fiber debonding increases towards the fiber embedded end (Phase 1). The deformation of the fiber is a result of elastic deformation of the debonded fiber part and the free fiber length as Redon et al.[39] state. Second, the pull-out force drops significantly when the bond between the fiber and the cementitious matrix is broken (Phase 2). Last, the fiber is fully debonded and the embedded end starts to move in the pull-out direction (Phase 3). The resulting load is caused by frictional forces. Fiber sliding is influenced by either slip-hardening, constant friction, or slip-softening phenomena. The slip phenomena can be described by an individual slip coefficient β.[40] The slip phenomena of the fiber depends on its hardness compared to the matrix. A slip-hardening effect is expected for polymeric fibers as fiber parts are peeled off the softer fiber surface, which then block the extraction. This results in an increase of the pull-out force (jamming effect). The model presented here neglects the difference between a first linear elastic behavior of the interface and the following start of debonding, as it was observed by Singh et al.[41] In practical tests the phases of SFPT are often not clearly seen as shown in Figure 1. However, a precise determination of the specific transition points between the different phases is essential to evaluate adhesion modifications on the fiber-matrix system. Different attempts have been made to clearly determine the transition points between the different phases.[41]

Alberti et al.,[27] Hofmann et al.[42] and Pecce et al.[43] placed a fiber in a concrete block in the way that the fiber movement at the free end can be measured by linear variable differential transformers (LVDTs). This setup allows correlating fiber movement and resulting force. Babafemi et al.[44] analyzed a creep pull-out with x-ray computed

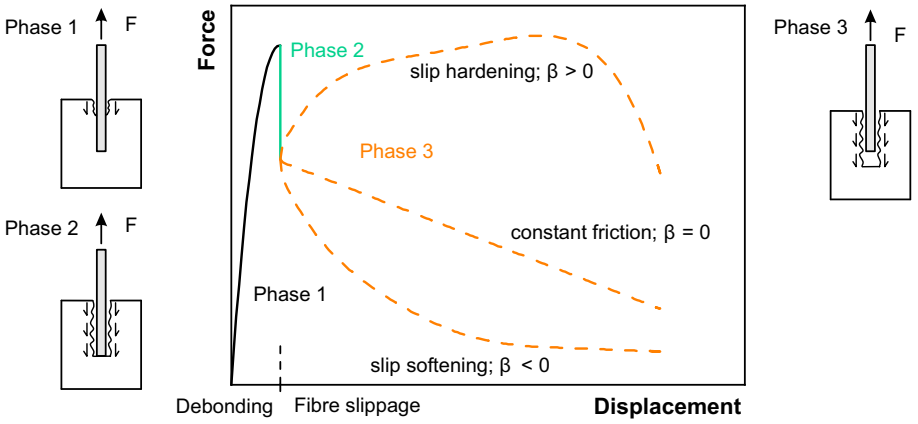

FIGURE 1 Idealized pull-out behavior of polymer fibers according to Redon et al.[39]

TABLE 1 Polymer properties of fiber materials.

	PP	PP-*g*-VTES	PET	PEEK
Processing temperature (°C)	190–250	170–230	270–290	380–400
Density (g/m^3)	0.905	0.905	1.400	1.300
Crystallinity	Semi	Semi	Semi	Semi
Polarity	Non-polar	Polar	|Polar	|Polar
Surface energy (mN/m)	29.68 ± 1.95	29.21 ± 1.34	42.30 ± 4.34	48.90 ± 2.10
Dispersive part (mN/m)	29.66 ± 1.86	27.76 ± 0.98	38.10 ± 2.50	43.60 ± 1.30
Polar part (mN/m)	0.03 ± 0.09	1.44 ± 0.35	4.20 ± 1.90	5.40 ± 0.90
Maximum draw ratio	1:17	1:11	1:07	1:3.5
Young's modulus (MPa)	12,128 ± 1011	3554 ± 290	13,347 ± 686	8679 ± 194
Tensile strength (MPa)	573 ± 46	216 ± 29	594 ± 32	527 ± 16
Strain (%)	6.44 ± 0.95	7.79 ± 0.96	6.42 ± 0.22	9.84 ± 0.38

tomography (CT) and were able to visualize the fiber movement. Hüsken et al.[45] used CT as well as acoustic emission (AE) analysis to understand the failure mechanism of steel fiber reinforced concrete. The AE analysis was also used by Pottmeyer et al.,[46] Di et al.[2] and Abouhussien et al.[47] for pull-out tests of steel reinforcement bars from concrete to determine the point of failure.

In this study, the debonding mechanism of fibers from different polymers as well as chemically modified PP were tested in SFPT. A modified SFPT was developed to further investigate the debonding mechanism in SFPT of the polymer fibers, which is characterized by different deformation behavior. A fully elastic behavior is expected in Phase 1, whereas Phase 2 is characterized by a distinct and sudden load drop. It is assumed that the beginning debonding is accompanied by acoustic emission. Therefore, AE sensors were placed at the surface of the test specimen to identify the characteristic points in SFPT. The transition from Phase 2 to Phase 3 is characterized by complete fiber movement and fiber deformations. Fiber movements were determined using a LVDT at the free end of the fiber, whereas deformations of the fibers were measured by Digital Image Correlation (DIC). The results of AE measurements were correlated with pull-out force, fiber movement (LVDT) and deformation measurements (DIC).

2 | EXPERIMENTS

2.1 | Materials

The fibers were produced out of four different polymeric materials with varying polarity, mechanical properties, and adhesion ability to the concrete matrix. Further properties are given in Table 1. A polypropylene (PP) with a Melt Flow Index (MFI) of 1 dg/min as standard material for fiber reinforced concrete was used as reference. The same PP was modified by side chain grafting via reactive extrusion with a vinyltriethoxysilane (PP-*g*-VTES) to increase the bonding behavior to the matrix. The reactive extrusion was carried out as described by Felix et al.[16] For representing an engineering polymer, Polyethylene Terephthalate (PET) was chosen due to its higher mechanical properties, polarity and possible chemical interaction with the cementitious matrix. Polyether ether ketone (PEEK) is a high-performance polymer with good mechanical properties as well as a good bond behavior to the cementitious matrix as shown by a previous study.[28]

2.2 | Fiber draw down

A HAAKE polydrive single screw extruder with screw diameter of 19 mm and a length/diameter ratio of 25 as well as a Dr. Collin MDO laboratory machine with a take-up speed of 3 m/min were used for fiber production. The pre-dried polymer granulates were extruded to a strand with a diameter of approximately 3 mm. The strand was drawn down at an oven temperature of 20 °C below the crystallite melt temperature of each polymer using two draw godets with different speed. The strand is stretched due to the higher speed of the second roller package. The draw ratio is defined as the ratio of the differing godet speeds. A schematic overview of the fiber draw down process is shown in Figure 2.

2.3 | Specimen preparation

The specimen preparation and the fiber embedding is shown in Figure 3. The fibers were cleaned with ethanol and placed through the mold, which measured

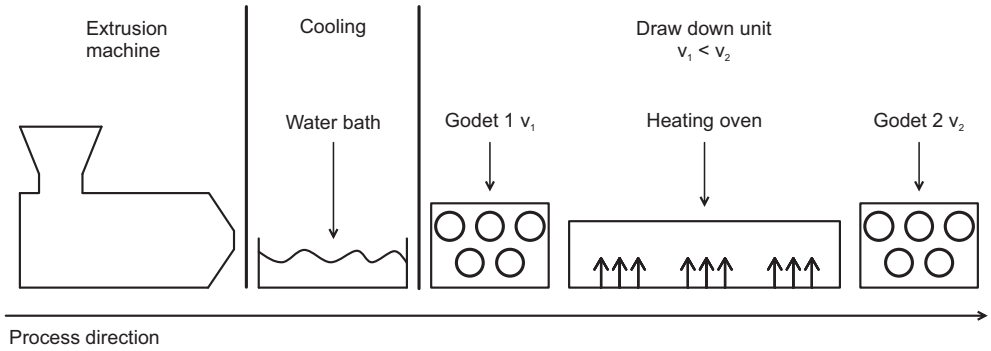

FIGURE 2 Schematic description of fiber draw down process.

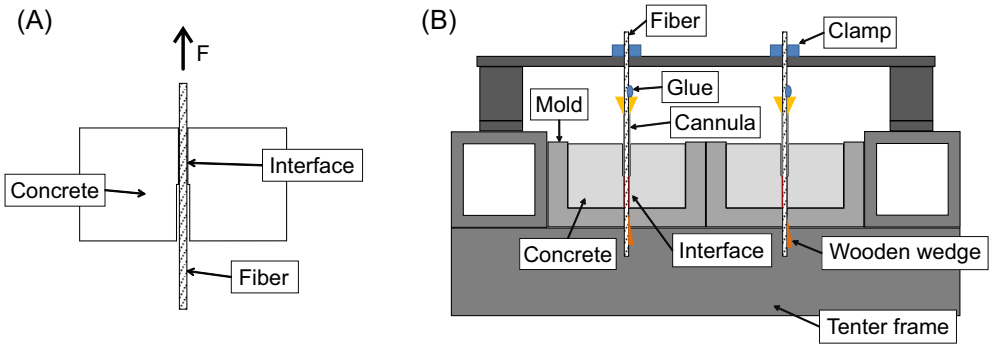

FIGURE 3 Fiber embedding and specimen preparation: (A) specimen cross section with embedded fiber; (B) specimen preparation and casting.

TABLE 2 Mix proportining of the mortar mix used.

Material	Sand	CEM I 52.5 N	Limestone Powder	Water	Superplasticizer Type 1	Superplasticizer Type 2
Amount (g)	1350	450	75	220	6.15	3.04
Amount (wt%)	64.2	21.4	3.6	10.5	0.29	0.14

$60 \times 60 \times 30$ mm. The fiber was pinned by a wooden wedge at the bottom and clamped on the top to achieve a straight fiber embedding. The contact length between fiber and concrete was set to 15 mm. After placing the fibers, mortar was poured into the mold. After 24 h the specimens were detached from the mold and placed in water, which was kept at constant temperature at 20 °C for additional 13 days. Before testing on the 15th day after production, the specimens were dried for 24 h at 60 °C to avoid AE-signals caused by the drying process.

The composition of the mortar used is listed in Table 2. The mortar was mixed according to the requirements given in DIN EN 196-1.[48] The mortar consists of sand (CEN Standard sand[48]), ordinary Portland cement (CEM I 52.5 N) and limestone powder. Two superplasticizers were used to control the viscosity and workability of the mortar.

2.4 | Contact angle measurements

As mentioned before, the chemical activity and polarity of the used polymers is of vital importance to understand the adhesion mechanisms of fibers embedded in concrete. With contact angle measurements, the polarity of each fiber can be determined by the method of Owen, Wendt, Rabel and Kaelble (OWRK-method).[49] Drops of two different liquids, water and diiodomethane, were placed on the dried and cleaned fiber and the contact angle was measured. The disperse and polar part of the surface energy can be calculated by the OWRK-method from the resulting contact angle. For this test a Krüss EasyDrop FM40 was used.

2.5 | Mechanical testing

The mechanical properties correlate with the fiber-matrix adhesion.[28] A universal testing machine (Zwick Z100) equipped with 90° deflection grips and a 10 kN load cell was used to test the mechanical properties of the fibers. The tests were performed according to DIN EN 14889-2[15] and DIN EN ISO 2062.[50] The Young's modulus was measured with 1 mm/min cross head displacement in the strain area of 0.05%–0.25%. Afterwards the strain rate

was increased to 10 mm/min until fiber rupture to measure the tensile strength.

2.6 | Single fiber pull-out tests

The results of the SFPT and the corresponding sensor data allow to determine an individual bond strength τ for each part in the SFPT. The bond strength is calculated as follows:

$$\tau = \frac{F}{\pi l_e D}, \quad (1)$$

whereas F is the force at a certain position in the force-displacement diagram, l_e describes the embedded fiber length and D the fiber diameter.

According to Figure 1, each phase can be determined and the specific bond strength for each transition point expresses the bonding mechanism. The transition from Phase 1 to Phase 2 marks the beginning of complete fiber movement in the concrete block and the end of chemical bonding and mechanical anchoring by embossments or undercuts resulting from the fiber roughness. In addition, the fiber-matrix interface is changing from an elastic to a plastic strain behavior. The end of Phase 1 marks the maximum force of the SFPT. At this point, a combination of chemical bonding and mechanical anchoring is paired with friction between the fiber and the mortar resulting from the already broken fiber-matrix interface. Full fiber debonding exists in Phase 2. After this point only friction is assumed to act in the SFPT (Phase 3).[39,51,52]

Roughened PP and PP-*g*-VTES fibers were tested additionally to evaluate the influence of mechanical anchoring and increased surface area in the SFPT. The fibers were roughened by adding them into the dry concrete constituents (sand, gravel) and mixed for 4 min. Afterwards, the fibers were extracted, washed with ethanol, air dried, and tested by SFPT.

2.6.1 | Test set-up

Single fiber pull-out tests were conducted to characterize the pull-out process and the bond behavior of the different fiber types. The tests were performed using a universal testing machine with a crosshead speed of 1 mm/min. A calibrated force cell with maximum capacity of 1 kN was used to allow precise measurements of the pull-out forces. Two linear variable differential transformers (LVDTs) were used to measure on the one hand the total fiber pull-out (LVDT_Clamping) on top of the sample and on the other hand the fiber movement at the free end at the bottom of the embedded fiber (LVDT_Fiber). Furthermore, the fiber pull-out was observed by digital image correlation (DIC) and acoustic emission (AE) analysis. A detailed overview of the test set-up is provided in Figure 4.

Deformations of the fibers between the clamping and the upper surface of the specimen were measured by the DIC system using reference points having a diameter of 0.4 mm. The optical deformation measurements were performed using an ARAMIS Adjustable Base 12 M system supplied by GOM, Gesellschaft für optische Messtechnik mbH. The measuring volume was set to $85 \times 65 \times 45$ mm (width × height × depth). Pictures were taken with variable rate between xx and xx frames per second. Figure 5 shows the denomination of the reference points used. Deformations (d) were measured in the direction of the applied pull-out force for single points (Fiber_1 [DIC], Fiber_2 [DIC]) or averaged deformation (avg(d)) for point arrays (Clamping [DIC], Support [DIC]). Furthermore, the deformation (ΔL_Fiber [DIC]) between the single points Fiber_1 (DIC) and Fiber_2 (DIC) was calculated from the DIC data. Additionally, the measured force and the piston displacement of the testing machine was transmitted to the DIC system by a voltage signal and recorded by the DIC system for every picture. The DIC system was calibrated before the fiber pull-out tests.

Four acoustic emission sensors (VS150MS) were fixed to the specimen laterally and acoustically coupled using viscoelastic adhesive pads BosticPrestik®. The acoustic emission signals were processed and stored by an AMSY6 acoustic emission system supplied by Vallen Systeme GmbH. The detection threshold was set to 28.3 dB_{AE} and the bandpass filter was set to 25–800 kHz for all sensors. No additional filter was applied for signal analysis. Every single point in the corresponding diagrams represents a single hit on one of the AE sensors.

3 | RESULTS AND DISCUSSION

3.1 | Mechanical properties

The mechanical properties determined by tensile tests are listed in Table 1. However, it must be considered that these properties were achieved by drawing each fiber to its individual maximum draw ratio and the maximum chain orientation, respectively. Drawn PET fibers show a tensile strength of 590 MPa and a Young's modulus of 13.3 GPa. The Young's modulus of PP fibers is 12.2 GPa and their tensile strength is with 573 MPa within the standard deviation of PET fibers. It was not possible to draw PEEK fibers to the same draw ratio as PP or PET

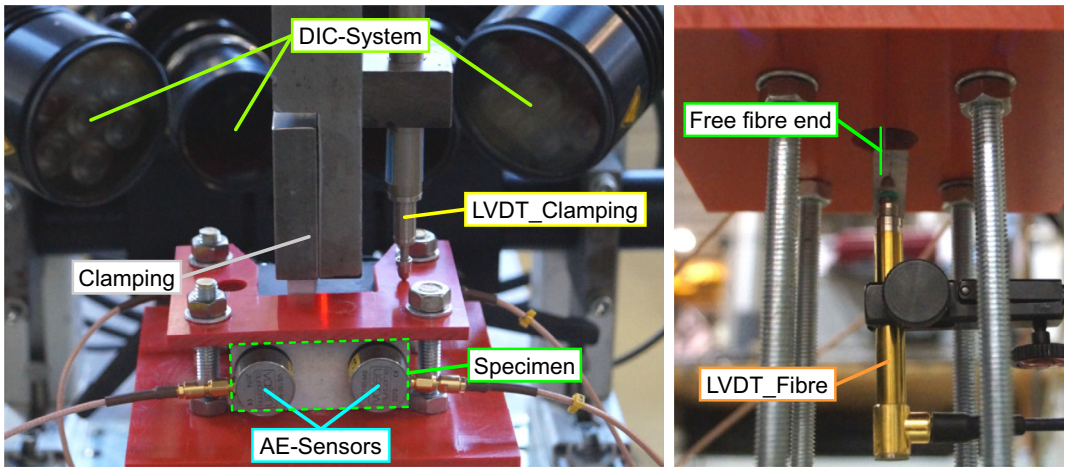

FIGURE 4 Test set-up of single fiber pull-out tests.

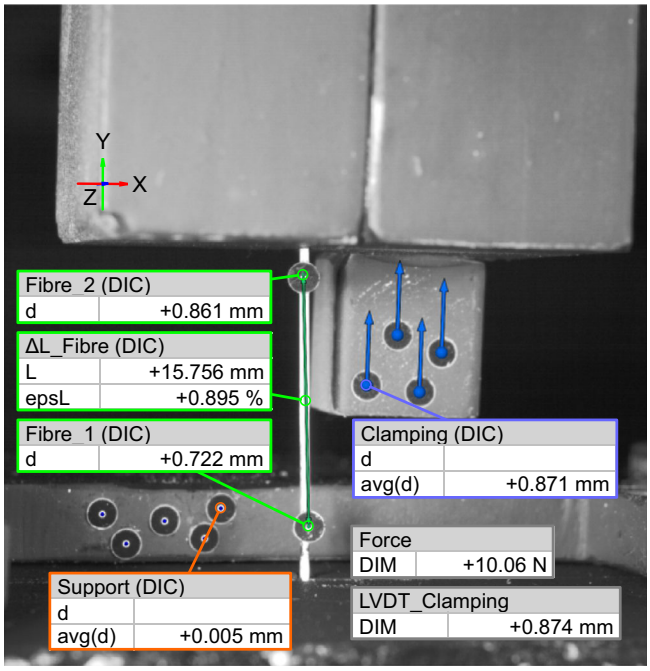

FIGURE 5 Relevant data obtained from the Digital Image Correlation (DIC) measurements.

due to the chemical structure of PEEK. However, as the maximum draw ratio of PEEK fibers is 1:3.5, the fibers show a high tensile strength of 527 MPa and a Young's modulus of 8.7 GPa. In comparison, fibers drawn from PP-*g*-VTES show low mechanical properties with a tensile strength of 216 MPa and a Young's modulus of 3.6 GPa. The low mechanical properties of PP-*g*-VTES fibers are caused by the low molecular weight of the polymers. In the reactive extrusion, the peroxide decreases the molecular chain length. A low molecular weight leads to lower tensile strength and Young's modulus as reported by Flood et al.,[53] Misra[54] and Capaccio et al.[55]

It was shown in a previous study[28] that the Young's modulus correlates with the bond strength calculated from SFPT. Hampe et al.[51] propose that a mismatch in the elastic moduli between the fiber and the matrix decreases the force distribution. A low force distribution leads to stress concentrations on the fiber entry side and the fiber end.[56] Predicting the bond strength by using the results obtained from the mechanical tests, PP and PET fibers should reach the highest bond strength followed by PEEK.

3.2 | Surface energy

The polarity on each fiber's surface can be determined by analyzing the surface energy. The corresponding values are given in Table 1 and can be correlated with the results of the SFPT. PEEK is the most polar material in this series. PET fibers can be considered as polar with a value of 4.20 mN/m measured for the polar part in contact angle measurements. The polarity of PET fibers results from the ester functional groups in the polymer. Grafting PP with VTES results in an increase of the polarity from 0.03 to 1.44 mN/m. These results correspond to the chemical structure of each polymer. The low influence on the polarity of silane functional groups on PP can be explained by the low amount of about 5 wt% of silane in the compound. The surface energy in total is not changed within the PP-g-VTES. A high polarity of the fiber increases the bond to the cementitious matrix via hydrogen bonds.[57] In addition, a high polarity leads to a better wetting of the fiber surface with the polar concrete matrix. Good wetting behavior of the fiber surface with the cement paste of the concrete results in a better fiber-matrix bonding.[58]

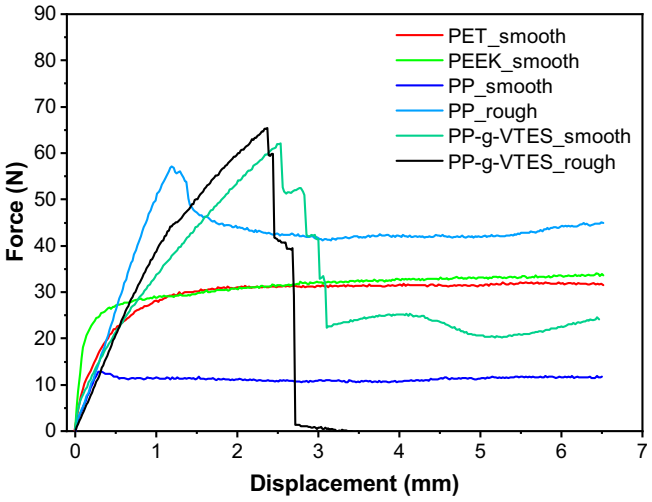

FIGURE 6 Averaged pull-out curves for the tested fiber materials.

3.3 | Single fiber pull-out tests

The maximum force obtained at the end of Phase 2 (Figure 1) is used to calculate the corresponding bond strength according to Equation (1). The average pull-out force for each tested fiber material is shown in Figure 6 and the corresponding bond strength is depicted in Figure 9 as Max_Phase_2. It is worth mentioning that it was not possible to perform a real pull-out test due to the free fiber end and the fibers were, therefore, pulled through the specimen.

As shown in a previous study, the bond strength increases for roughened fibers[28] as the resulting undercuts improve the mechanical anchoring of the fibers in the cementitious matrix. Mechanical anchoring is also improved by crimping or embossment as shown by Kaufmann et al.[59] These geometrical or surface defects increase the force needed to pull-out the fiber from the matrix as a slightly thicker part of the fiber must be pulled through a thinner fiber channel of the hardened matrix. This effect was demonstrated in a previous study[28] for all tested fibers. However, it was not possible to determine higher bond strength for the roughened PP-*g*-VTES fibers. All roughened PP-*g*-VTES fibers failed by fiber rupture in SFPT and a complete fiber pull-out was not possible. The early fiber failure is a result of the low tensile strength of the roughened PP-*g*-VTES fibers. Therefore, smooth and roughened PP-g-VTES fibers show the same bond strength. This leads to the conclusion that a roughened PP-*g*-VTES fiber with higher tensile strength might result in higher bond strength, if fiber rupture is avoided.

Comparing all smooth fibers, PP fibers without any modification show the lowest bond strength followed by PEEK fibers with a slightly higher bond strength. This allows for the conclusion that the polarity of the fibers does not influence their bond strength significantly. Ester saponification on the surface of PET fibers is a possible cause for the higher bond strength compared to PP. Furthermore, the higher stiffness results in a better load distribution along the fiber. The highest bond strength of smooth fibers was achieved by the silane modified PP fibers. The ethoxy groups of the VTES grafted PP can react with reaction products of the cement hydration, for example, the C-S-H phases, and create a covalent bond between the PP-*g*-VTES fiber and the cementitious matrix via siloxane bridges (Si—O—Si).

These Si—O—Si bonds result in improved bond between the fiber and the cementitious matrix.[60,61] The insufficient mechanical properties of the fibers can be overcome by the covalent bonded fibers. Zhou et al.,[62] Wu et al.[63] and Shi et al.[57] demonstrated a similar effect with silane coatings applied on different fiber types that were embedded in a concrete matrix. In another study on silane coatings, Casagrande et al.[64] postulated that the pull-out energy is increased with tetraethoxysilan, which is chemically comparable to the VTES used in this study. However, all these results do not give further insights into the debonding mechanisms. It is not known whether the polarity of the fibers or the silanization influences Phase 1 or Phase 2. Therefore, it is also possible that the increased surface roughness contributes in Phase 3 and increases the resistance against fiber pull-out after full fiber debonding.

3.3.1 | Characterization of debonding mechanism

Figure 7 shows selected plots for the SFPTs performed on the different polymer fibers used in this study. Figure 8 shows the same data as Figure 7, but the focus is on the transition of Phase 2 to Phase 3. The sub-plots of Figure 7 and Figure 8 contain the resulting pull-out force, the total fiber pull-out (LVDT_Clamping), the fiber movement (LVDT_Fiber) measured by a LVDT at the free end of the embedded fiber (see Figure 3), the displacement of two measuring points (Fiber_1 (DIC), Fiber_2 [DIC]) and the resulting deformation (ΔL_Fiber [DIC]) between the two measuring points of the fiber during fiber pull-out (Figure 5). By correlating the pull-out force with the fiber movement (LVDT_Fiber), the transition from Phase 2 to Phase 3 can be identified for each tested specimen. A fiber movement at the free end of the fiber occurs when the fiber is fully debonded. According to Redon et al.[39] a fully debonded fiber shows only frictional bond when the maximum pull-out force is reached at the end of Phase 2. It can also be assumed that the fiber-matrix interface and the resulting bond between the fiber and

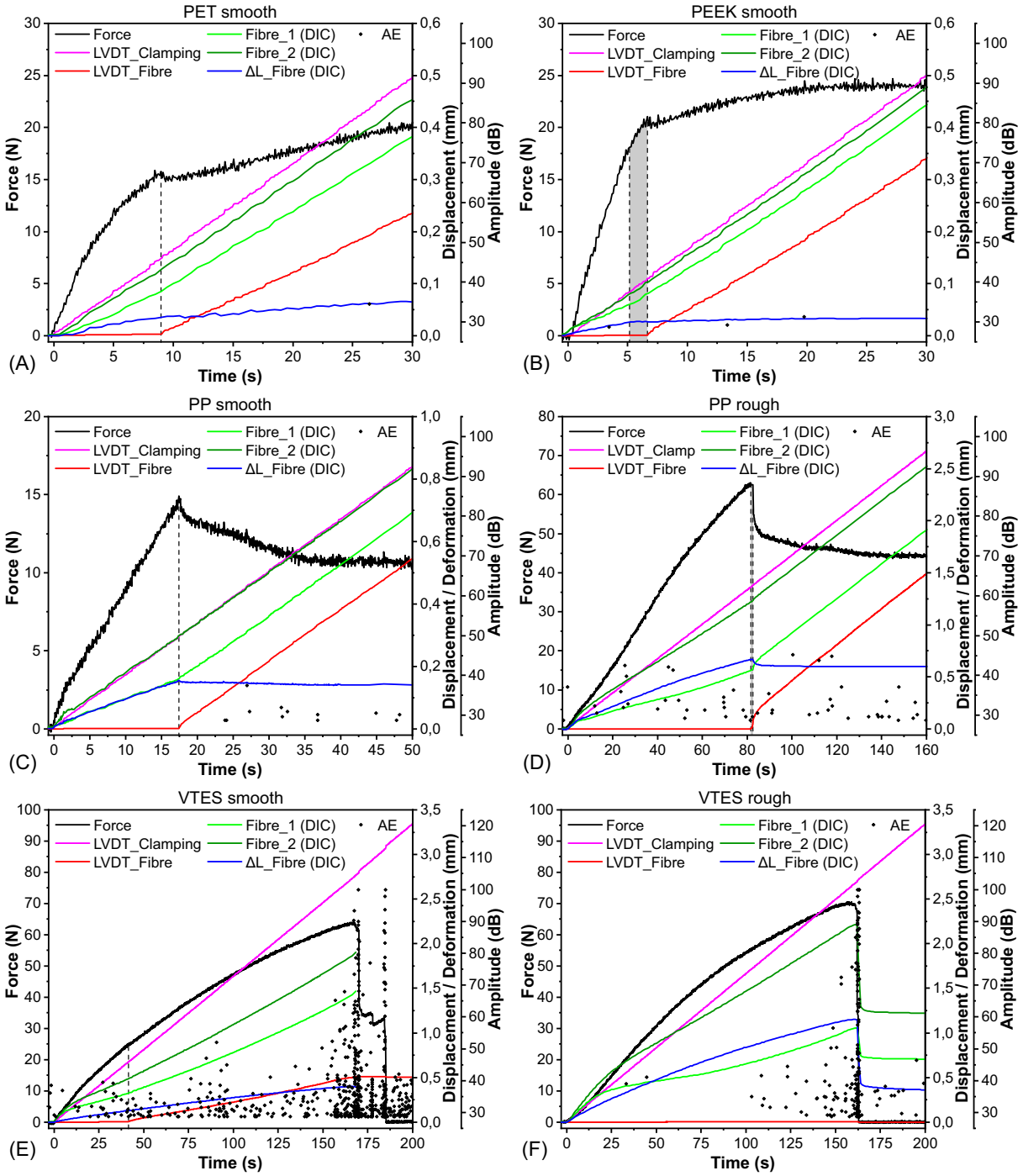

FIGURE 7 Measured data of the single fiber pull-out test (SFPT): (A) polyethylene terephthalate (PET) smooth; (B) polyether ether ketone (PEEK) smooth; (C) polypropylene (PP) smooth; (D) PP rough; (E) vinyltriethoxysilane (VTES) smooth; (F) VTES rough.

the cementitious matrix is destroyed when the fiber is fully debonded.

The results of a smooth PET fiber are shown in Figure 7A and Figure 8A. The force increases and reaches a first maximum at about 15 N. After the first maximum is reached, the force decreases slightly, followed by a further increase that reaches a constant value for large fiber pull-out. A fiber movement due to complete debonding of the fiber can be seen at about 8.9 s (LVDT_Fiber). The detected movement of the fiber corresponds to the first force maximum at about 15 N. A similar effect can be seen in Figure 7B for the smooth PEEK fiber. The force increases until a first maximum is reached at about 21 N. However, the force decrease after the first maximum is not that distinct for the PEEK fiber as for the PET fiber, but the pull-out force also increases with increasing fiber

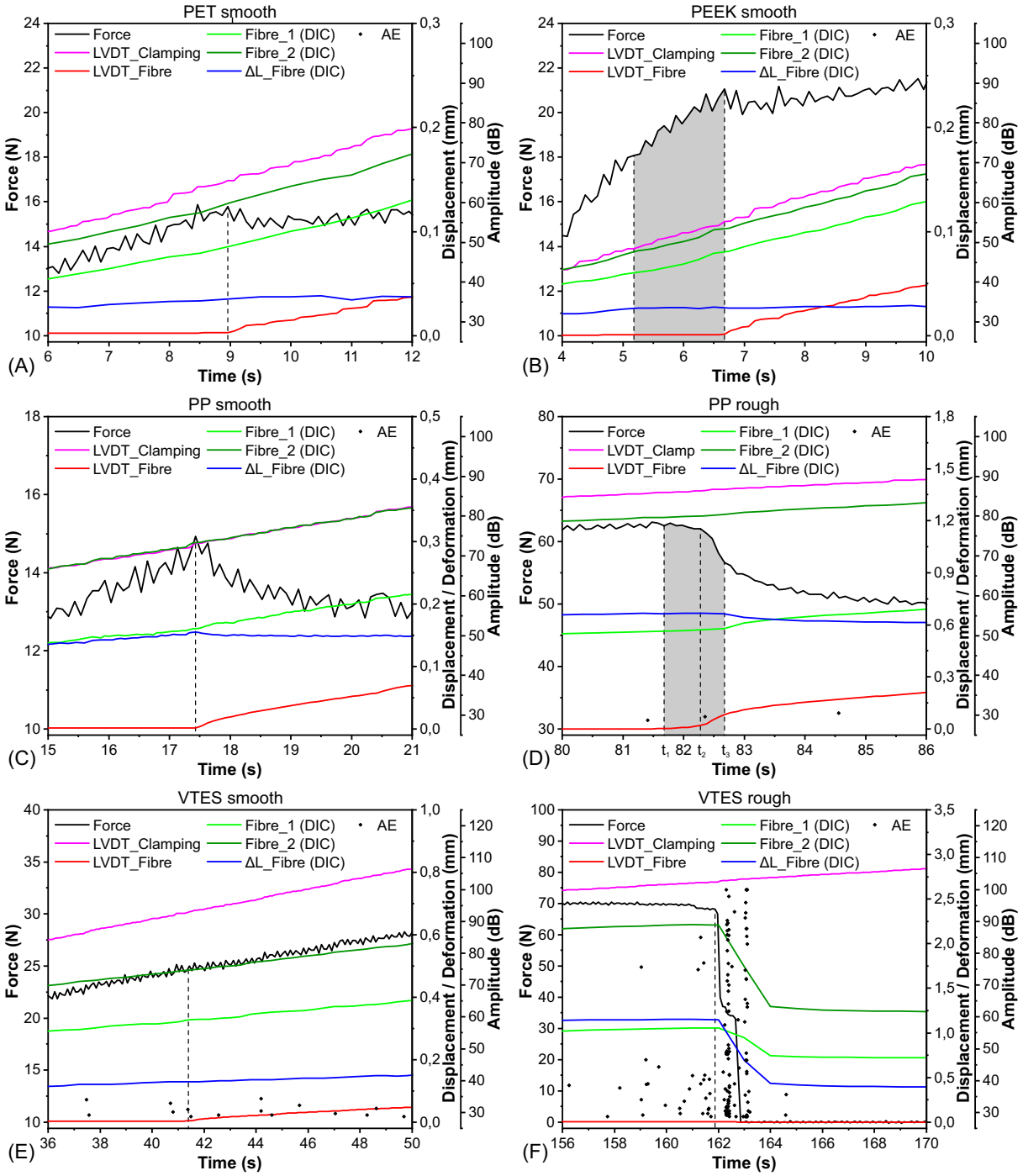

FIGURE 8 Measured data of the single fiber pull-out test (SFPT) around the transition of Phase 2 to Phase 3: (A) polyethylene terephthalate (PET) smooth; (B) polyether ether ketone (PEEK) smooth; (C) polypropylene (PP) smooth; (D) PP rough; (E) vinyltriethoxysilane (VTES) smooth; (F) VTES rough.

pull-out until a constant value is reached. A fiber movement is indicated by the LVDT_Fiber at about 6.7 s, which also corresponds to the first force maximum at about 21 N.

Even though PET and PEEK fibers show similar pull-out behavior, the deformation behavior of the fibers measured by the DIC system differs. The deformation ΔL_Fiber (DIC) of the PET fiber increases until the first force maximum is reached. The fiber deformation ΔL_Fiber (DIC) is governed by the Young's modulus of the fiber. After reaching the first force maximum at about 8.9 s, the pull-out force decreases slightly, followed by a further increase. The further increase of the pull-out force causes an increase of the fiber deformation, but the

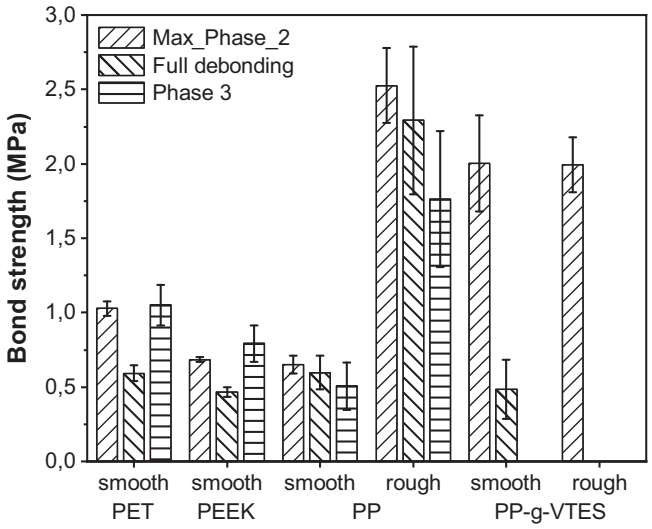

FIGURE 9 Calculated bond strength for different debonding criteria.

slope of the corresponding curve ΔL_Fiber (DIC) is lower. The PEEK fiber shows a different deformation behavior during fiber pull-out. Here, the deformation of the fiber stops at about 5.2 s, while the first force maximum is reached at about 6.7 s. The resulting difference in time is marked by the gray area in Figure 7B and Figure 8B, respectively. Considering the data of the DIC system, the PEEK fiber shows no significant fiber deformations after 6.7 s although the pull-out force is increasing. This indicates a different debonding mechanism for the PEEK fiber compared to the one of PP and PET fibers, which might be caused by a higher polarity of the PEEK fiber. Significant acoustic events that can be correlated to the debonding mechanism of the fiber pull-out of PET and PEEK fibers were not recorded.

The sub-plots *c* and *d* of Figures 7 and 8 show the results obtained for smooth and roughened PP fibers. The pull-out force increases for both fiber types as described by Redon et al.[39] and shows a distinct drop after reaching the maximum and before the pull-out force is constant in Phase 3. Fiber movement is indicated by the LVDT_Fiber for both fiber types when the maximum force is reached. However, both the maximum force and the force decrease differ for smooth and roughened PP fibers. Roughened PP fibers have a higher bond strength due to the better mechanical anchoring and result, therefore, in a higher pull-out force.

The data obtained by the DIC measurements show also the difference in the transition from Phase 1 to Phase 2 for smooth and roughened PP fibers. The deformation ΔL_Fiber (DIC) of the smooth PP fiber correlates with the pull-out force and increases with increasing fiber pull-out until the fore maximum is reached at about 17.4 s and decreases slightly after reaching the maximum. The deformation ΔL_Fiber (DIC) and the pull-out force of the smooth PP fiber are constant with increasing fiber pull-out in Phase 3. The roughened PP fiber shows a different deformation behavior after reaching the maximum pull-out force that is characterized by three noticeable points denominated with t_1–t_3 in Figure 8D. Here, the fiber deformation ΔL_Fiber (DIC) also increases with increasing pull-out force until the force maximum is reached at about 81.7 s (t_1) and fiber movement is indicated by the LVDT_Fiber. However, the pull-out force decreases slightly with increasing fiber pull-out until t_2 is reached at about 82.3 s and shows a significant decrease after t_2. The same fact holds for the fiber movement LVDT_Fiber, which shows a slight increase between t_1 and t_2 and a significant increase after t_2 is reached. The fiber movement LVDT_Fiber stabilizes after t_3 is reached at about 82.7 s. The fiber deformation ΔL_Fiber (DIC) also decreases slightly after t_3 is reached. It is worth mentioning that this decrease of the fiber deformation ΔL_Fiber (DIC) is related to the elastic part of the total fiber deformation and is caused by the decreased pull-out force. This effect is also evident when the displacement of the measuring points Fiber_1 (DIC) and Fiber_2 (DIC) is analyzed. The upper measuring point Fiber_2 (DIC), which is closer to the clamping of the fiber (cf. Figure), shows the same displacement as the clamping (LVDT_Clamp), but the lower measuring point Fiber_1 (DIC), which is closer to specimen surface, shows a larger displacement that is comparable to the fiber movement LVDT_Fiber.

Significant acoustic events that can be correlated to the debonding mechanism of the fiber pull-out of the smooth PP fibers were not recorded. A low number of acoustic events was detected for the smooth PP fiber after the maximum pull-out force was reached and fiber movement was detected by the LVDT_Fiber. However, owing to the low number of acoustic events and their low amplitude, it is not possible to clearly relate these acoustic events to the mechanisms of Phase 3 that are governed by frictional forces. Although a higher number of acoustic events was recorded for the roughened PP fiber during fiber pull-out, it is also not possible to clearly relate these acoustic events to the specific phases of fiber debonding due to their low amplitude and the fact that two of these events were recorded before the fiber pull-out was started.

The results shown for both PP-g-VTES fiber types in Figure 7 and Figure 8 reveal a different pull-out behavior, as the fibers ruptured during the pull-out test. Fiber rupture was accompanied by a high number of high-amplitude acoustic emission signals for both fiber types. The increase of acoustic emission activity before

complete or partly fiber rupture might be attributed to single ligament ruptures. However, a fiber movement was detected at about 41.4 s by the LVDT_Fiber for the smooth PP-*g*-VTES fiber, which is not accompanied by a decrease in the pull-out force. It was not possible to achieve a complete debonding of the roughened PP-*g*-VTES fiber with fiber movement (LVDT_Fiber), as the tensile strength of the PP-*g*-VTES fiber is too low. Therefore, it is assumed that a PP-*g*-VTES fiber with higher tensile strength will also result in higher pull-out forces.

The data of the DIC measurement show that deformation ΔL_Fiber (DIC) of both fibers increases until the maximum force is reached before fiber rupture. The fiber rupture is accompanied by a high acoustic activity, characterized by a larger number of acoustic events with high amplitudes. The smooth PP-*g*-VTES fiber shows also a large number of acoustic events during the pull-out and before fiber rupture. However, some of these acoustic events with low amplitude were recorded before the fiber pull-out was started. The roughened PP-*g*-VTES fiber shows almost no acoustic activity during fiber pull-out and first acoustic events with amplitudes $> 40\ dB_{AE}$, which indicate the fiber rupture, were recorded before the maximum force was reached.

The results of the SFPT demonstrate that the transition from Phase 2 to Phase 3 can be identified by displacement measurements (LVDT_Fiber) at the free end of the embedded fiber, while it is not possible to clearly identify this transition point from conventional force-displacement diagrams (cf. Figure 6). The point of full debonding identified by LVDT_Fiber is identical to the first maximum value in the force-displacement curve of PET, PEEK and PP fibers (cf. Figure 7). Translated to the VTES fiber, where the first maximum value in the force-displacement curve is not clearly detectable, the transition from Phase 2 to Phase 3 can be identified by the increase of the LVDT_Fiber curve. Therefore, it can be assumed that VTES fibers have a different debonding mechanism compared to other fiber types, due to a mechanical plugging by abraded fiber particles. Furthermore, the test results presented in Figure 7 reveal polymer specific effects that occur during the SFPT. PET and PEEK fibers show similar pull-out behavior. Both materials show a slight drop in the pull-out force at the end of Phase 2, which is followed by a further increase with increasing fiber pull-out in Phase 3. The clear identification of this transition point and the related complete debonding from the force-displacement plots of standard SFPT is not possible for PET and PEEK fibers (cf. Figure 6).

The recorded pull-out forces are governed in Phase 3 by frictional forces as stated by Redon et al.[39] and Li and Stang.[65] Figure 6 reveals the difference between the non-polar PP fiber and the polar PET and PEEK fibers. While the PP fibers show a pull-out behavior as described in the literature with a drop of the pull-out force before reaching a constant value due to frictional forces.[27,44] PET and PEEK fibers show no significant drop in their pull-out force and remain at a constant or slightly increasing level with the maximum pull-out force even in Phase 3. This fact can be attributed to the higher surface roughness or a higher resistance of the fiber surface to be sheared-off by the surrounding cementitious matrix.[28] Higher bond strength can be achieved by better mechanical anchoring due to fiber roughening or embossment as stated by Behfarnia et al.[66] or Babafemi et al.[34]

The highest pull-out force was determined for PP-*g*-VTES fibers. Smooth and roughened PP-*g*-VTES fibers ruptured at about 60 N and debonding mechanism cannot be seen in the force-displacement curves. However, by measuring the fiber movement at the free end it was demonstrated that complete debonding occurs at about 25 N for smooth PP-*g*-VTES fibers. Furthermore, the fiber roughening leads to higher strength of the fiber-matrix interface due to a larger fiber surface and, consequently, a higher amount of covalent bonds by siloxane bridges is assumed. A fiber debonding was not detected for rough PP-*g*-VTES fibers as a corresponding movement was not measured by the LVDT_Fiber. Additionally, PP-g-VTES fibers overcame the negative influence on the bond by their low mechanical properties as described by Marotzke.[56] It is assumed that a higher Young's modulus leads to a higher bond strength.

Different bond strength values can be calculated for the data of the SFPT performed in this study. The maximum bond strength depicted in Figure 9 was calculated from data obtained by a regular analysis of SFPT. Figure 9 reveals that all smooth fibers show comparable bond strength ranging from 0.47 to 0.60 MPa when a full debonding of the fiber is considered. This effect was not expected for the PP-*g*-VTES fibers as these fibers were developed to show a higher chemical bond that contributes to Phase 1. It can be concluded that different polymer types and fiber modification show no significant effect on the bond strength at the point of full fiber debonding. The modification of the SFPT set-up provides valuable information on the debonding mechanism, which helps to further engineer polymer fibers for concrete reinforcement.

4 | CONCLUSIONS

The pull-out behavior of different polymer fibers was investigated in this study by the SFPT and a modified test set-up was used to analyze the debonding mechanism of

the polymer fibers. This test set-up comprises a LVDT to measure the fiber movement at the free end of the embedded fiber as the movement of the fiber indicates a full debonding of the fiber from the surrounding cementitious matrix. Furthermore, the pull-out tests were accompanied by AE analysis and DIC. The following conclusions can be drawn from the results of this study:

1. Fiber movement measured at the free end of the embedded fiber indicates the full debonding of the fiber from the cementitious matrix and the damage of the fiber-matrix interface. The bond strength at full fiber debonding was calculated and gives more information on the debonding mechanism.
2. Different assumption were made for calculating bond strength values from the data of the SFPT. The bond strength values calculated for a full debonding of the fibers revealed that chemical modifications or the polarity of the fibers show no influence on the strength of the fiber-matrix interface in the first two phases of SFPT.
3. PP-*g*-VTES fibers show different pull-out behavior than the other tested polymer fibers. The point of full debonding of the other polymer fibers can be clearly identified by a combination of the first force maximum of the force-displacement diagram and displacement measurement at the free end of the embedded fiber. As PP-*g*-VTES fibers show no distinct point of full debonding in the force-displacement curve, full debonding can only be determined by corresponding displacement measurements at the free end of the embedded fiber.
4. Results obtained from standard SFPT suggest that PET, PEEK, and PP-*g*-VTES fibers show higher bond strength than PP fibers. The modified SFPT demonstrated that all polymers show comparable bond strength when a full debonding of the fiber is considered.
5. The roughening of the fibers improved the mechanical anchoring of the polymer fibers in the cementitious matrix, which resulted in higher bond strength and higher frictional forces after full debonding of the fiber.
6. It was not possible to record a sufficient number of acoustic events that can be correlated with the specific phases of fiber debonding. The few recorded events show a low amplitude that is slightly higher than the detection threshold of 28.3 dB_{AE}. Due to the low signal intensity and short signal length a detailed analysis of further signal features like average frequency, rise time or energy will not give useful information to describe the pull-out behavior. Therefore, it is not possible to relate the detected hits to friction induced processes during fiber pull-out. Potential signals related to pull-out mechanisms may have amplitudes and frequencies that are too low for detection with the applied sensors. However, acoustic events with higher amplitude were recorded for fiber rupture.
7. The four AE sensors were positioned near the edges of the specimen to cover the complete area of the specimen for acoustic event localization. However, due to the low signal amplitudes and the large sensor aperture (compared to the specimen size) the localization delivered insufficient results. Localization and signal analysis can be improved by using low frequency sensors and positioning of the sensors in the middle of the side surfaces of the specimen.

ACKNOWLEDGMENTS

The authors thank the German Federal Ministry of Education and Research for the financial support of this study through grant 13FH068PA6 and the Master Builders Solutions Deutschland GmbH for material samples. We express thanks to Prof. Leps of Rosenheim Technical University of Applied Sciences, Faculty of Wood Technology and Construction for his equipment support in mechanical tests. Open Access funding enabled and organized by Projekt DEAL.

ORCID

Michael Sigrüner https://orcid.org/0000-0002-0644-023X
Götz Hüsken https://orcid.org/0000-0002-1463-0308
Stephan Pirskawetz https://orcid.org/0000-0003-0626-5002
Jonas Herz https://orcid.org/0009-0006-7595-6711
Dirk Muscat https://orcid.org/0000-0002-6704-7343
Nicole Strübbe https://orcid.org/0000-0002-2084-9031

REFERENCES

[1] V. Afroughsabet, L. Biolzi, T. Ozbakkaloglu, *J. Mater. Sci.* **2016**, *51*, 6517.
[2] B. Di, J. Wang, H. Li, J. Zheng, Y. Zheng, G. Song, *Sensors* **2019**, *19*, 159.
[3] A. Brückner, R. Ortlepp, M. Curbach, *Mater. Struct.* **2006**, *39*, 741.
[4] L. N. Koutas, Z. Tetta, D. A. Bournas, T. C. Triantafillou, *J. Compos. Constr.* **2019**, *23*, 3118001.
[5] J. Kaufmann, K. Frech, P. Schuetz, B. Münch, *Constr. Build. Mater.* **2013**, *49*, 15.
[6] J. Rottstegge, C. C. Han, W. D. Hergeth, *Macromol. Mater. Eng.* **2006**, *291*, 345.
[7] M. M. Hilles, M. M. Ziara, *Eng. Sci. Technol.* **2019**, *22*, 920.
[8] T. Liu, H. Wei, A. Zhou, D. Zou, H. Jian, *Cem. Concr. Compos.* **2020**, *111*, 103638.
[9] Y. Xu, D. Chung, *Cem. Concr. Res.* **1999**, *29*, 1107.
[10] A. M. Brandt, *Compos. Struct.* **2008**, *86*, 3.
[11] L. Gu, T. Ozbakkaloglu, *Waste Manag.* **2016**, *51*, 19.

[12] T. K. M. Ali, *Environ. Dev. Sustain.* **2020**, *23*, 8433.
[13] A. Noushini, B. Samali, K. Vessalas, *Constr. Build. Mater.* **2013**, *49*, 374.
[14] N. Ranjbar, S. Talebian, M. Mehrali, C. Kuenzel, H. S. C. Metselaar, M. Z. Jumaat, *Compos. Sci. Technol.* **2016**, *122*, 73.
[15] DIN EN 14889-2, *Fibres for concrete. Part 2: Polymer fibres—Definitions, specifications and conformity (German version EN 14889–2:2006)*, Deutsches Institut für Normung e.V, Berlin **2006**.
[16] A. H. O. Felix, N. S. M. Cardozo, S. M. B. Nachtigall, R. S. Mauler, *Macromol. Mater. Eng.* **2006**, *291*, 418.
[17] M. Bengtsson, K. Oksman, *Compos. A: Appl. Sci. Manuf.* **2006**, *37*, 752.
[18] H. Huang, H. H. Lu, N. C. Liu, *J. Appl. Polym. Sci.* **2000**, *78*, 1233.
[19] S. M. B. Nachtigall, F. C. Stedile, A. H. O. Felix, R. S. Mauler, *J. Appl. Polym. Sci.* **1999**, *72*, 1313.
[20] S. Choi, S. Maul, A. Stewart, H. Hamilton, E. P. Douglas, *Polym. Eng. Sci.* **2012**, *53*, 283.
[21] F. Švegl, J. Šuput-Strupi, L. Škrlep, K. Kalcher, *Cem. Concr. Res.* **2008**, *38*, 945.
[22] D. Silva, A. Betioli, P. Gleize, H. Roman, L. Gómez, J. Ribeiro, *Cem. Concr. Res.* **2005**, *35*, 1741.
[23] S. Mishra, V. Zope, A. Goje, *Polym. Int.* **2002**, *51*, 1310.
[24] V. Popescu, A. Muresan, O. Constandache, G. Lisa, E. I. Muresan, C. Munteanu, I. Sandu, *Ind. Eng. Chem. Res.* **2014**, *53*, 16652.
[25] J.-P. Won, C.-G. Park, S.-J. Lee, J.-W. Kang, *J. Appl. Polym. Sci.* **2011**, *121*, 1908.
[26] A. M. López-Buenda, M. D. Romero-Sánchez, V. Climent, C. Guillem, *Cem. Concr. Res.* **2013**, *54*, 29.
[27] M. Alberti, A. Enfedaque, J. Gálvez, A. Ferreras, *Constr. Build. Mater.* **2016**, *112*, 607.
[28] M. Sigrüner, D. Muscat, N. Strübbe, *J. Appl. Polym. Sci.* **2021**, *138*, 50745.
[29] K. V. Pochiraju, G. P. Tandon, N. J. Pagano, *J. Mech. Phys. Solids* **2001**, *49*, 2307.
[30] Y. M. Abbas, M. I. Khan, *Arab. J. Sci. Eng.* **2016**, *41*, 1183.
[31] S. Zhandarov, E. Mader, *Compos. Sci. Technol.* **2005**, *65*, 149.
[32] M. Xie, V. M. Karbhari, *J. Compos. Mater.* **1997**, *31*, 1806.
[33] S. Abdallah, D. W. A. Rees, *Int. J. Concr. Struct. Mater.* **2019**, *13*, 27.
[34] A. Babafemi, W. Boshoff, *Constr. Build. Mater.* **2017**, *135*, 590.
[35] P. D. Maida, E. Radi, C. Sciancalepore, F. Bondioli, *Constr. Build. Mater.* **2015**, *82*, 39.
[36] Y.-C. Gao, Y.-W. Mai, B. Cotterell, *Z. Angew. Math. Phys.* **1988**, *39*, 550.
[37] C.-H. Hsueh, *Mater. Sci. Eng. A* **1990a**, *1*, 1.
[38] C.-H. Hsueh, *Mater. Sci. Eng. A* **1990b**, *67*, 67.
[39] C. Redon, V. C. Li, C. Wu, H. Hoshiro, T. Saito, A. Ogawa, *J. Mater. Civ. Eng.* **2001**, *13*, 399.
[40] Z. Lin, V. C. Li, *J. Mech. Phys. Solids* **1997**, *45*, 763.
[41] S. Singh, A. Shukla, R. Brown, *Cem. Concr. Res.* **2004**, *34*, 1919.
[42] S. Hofmann, N. L. Tran, T. Proske, C.-A. Graubner, *Struct. Concr.* **2020**, *21*, 2178.
[43] M. Pecce, F. Ceroni, F. A. Bibbò, S. Acierno, *Mater. Struct.* **2013**, *48*, 139.
[44] A. J. Babafemi, A. du Plessis, W. P. Boshoff, *Constr. Build. Mater.* **2018**, *174*, 466.
[45] G. Hüsken, S. Pirskawetz, D. Meinel, V. Babski, H.-C. Kühne, *Bautechnik* **2016**, *93*, 711.
[46] F. Pottmeyer, O. Schlegel, K. Weidenmann, M. Merzkirch, *Mater. Werkst.* **2018**, *49*, 1245.
[47] A. A. Abouhussien, A. A. A. Hassan, *Struct. Control. Health Monit.* **2016**, *24*, e1893.
[48] DIN EN 196-1, *Methods of testing cement—Part 1: Determination of strength; German version EN 196–1:2016*, Deutsches Institut für Normung e.V, Berlin **2016**.
[49] D. K. Owens, R. C. Wendt, *J. Appl. Polym. Sci.* **1969**, *13*, 1741.
[50] DIN EN ISO 2062, *Textiles—Yarns from packages. Determination of single-end breaking force and elongation at break using constant rate of extension (CRE) tester (ISO 2062:2009); German version EN ISO 2062:2009*, Institut für Normung e.V, Deutsches **2010**.
[51] A. Hampe, G. Kalinka, S. Meretz, E. Schulz, *Composites* **1995**, *26*, 40.
[52] S. Zhandarov, E. Mäder, C. Scheffler, G. Kalinka, C. Poitzsch, S. Fliescher, *Adv. Ind. Eng. Polym. Res.* **2018**, *1*, 82.
[53] J. E. Flood, S. A. Nulf, *Polym. Eng. Sci.* **1990**, *30*, 1504.
[54] S. Misra, F.-M. Lu, J. E. Spruiell, G. C. Richeson, *J. Appl. Polym. Sci.* **1995**, *56*, 1761.
[55] G. Capaccio, *Makromol. Chem.* **1981**, *4*, 197.
[56] C. Marotzke, *Compos. Sci. Technol.* **1994**, *50*, 393.
[57] F. Shi, S. Yin, T. M. Pham, R. Tuladhar, H. Hao, *Constr. Build. Mater.* **2021**, *277*, 122335.
[58] E. Wölfel, H. Brünig, I. Curosu, V. Mechtcherine, C. Scheffler, *Materials* **2021**, *14*, 722.
[59] J. Kaufmann, J. Lübben, E. Schwitter, *Compos. A: Appl. Sci. Manuf.* **2007**, *38*, 1975.
[60] J. Thomas, B. Joseph, J. P. Jose, H. J. Maria, P. Main, A. A. Rahman, B. Francis, Z. Ahmad, S. Thomas, *Ind. Eng. Chem. Res.* **2019**, *58*, 20863.
[61] H. Azizi, J. Morshedian, M. Barikani, *J. Vinyl Addit. Technol.* **2009**, *15*, 184.
[62] A. Zhou, Z. Yu, H. Wei, L. H. Tam, T. Liu, D. Zou, *ACS Appl. Mater. Interfaces* **2020**, *12*, 44163.
[63] Y. Wu, Q. Sun, H. Fang, W. Ren, F. Liu, *Compos. Interfaces* **2014**, *21*, 787.
[64] C. A. Casagrande, S. H. P. Cavalaro, W. L. Repette, *Constr. Build. Mater.* **2018**, *178*, 495.
[65] V. C. Li, H. Stang, *Adv. Cem. Based Mater.* **1997**, *6*, 1.
[66] K. Behfarnia, A. Behravan, *Mater. Des.* **2014**, *55*, 274.

How to cite this article: M. Sigrüner, G. Hüsken, S. Pirskawetz, J. Herz, D. Muscat, N. Strübbe, *J. Polym. Sci.* **2023**, 1. https://doi.org/10.1002/pol.20230264